ASCAT Ultrahigh-Resolution Wind Products on Optimized Grids

Jur Vogelzang and Ad Stoffelen

***Abstract*—The accuracy and spatial resolution of ultrahigh-resolution wind products derived from full-resolution ASCAT radar cross-section measurements are determined by the size and shape of the aggregation area. Current high-resolution products (ASCAT-coastal and ASCAT-6.25) are defined on a regular swath grid (size 12.5 and 6.25 km, respectively) and use a circular aggregation area (15 and 7.5 km radius resp.). For ASCAT-6.25, such approach leads to poor radar sampling, causing noise in the retrieved winds, and poor beam overlap, causing geophysical errors. More regular radar sampling and improved beam overlap can be obtained by using a grid that is synchronized with respect to the ASCAT mid-beam full-resolution measurements. This results in a new generation of ASCAT wind products. It is shown that a product on a 5.6 km grid size (on average) with optimized radar sampling compares better to buoys than ASCAT-6.25, but at the cost of an irregular grid and slightly degraded spatial resolution.**

***Index Terms*—Radar, wind.**

I. Introduction

STUDIES of dynamic mesoscale features over the ocean like convective cells, coastal jets, and von Kármán vortices in the wake of isles, require high-resolution wind data. Spaceborne scatterometers can provide such information. Recently, the ASCAT-6.25 product which contains ocean surface vector winds on a 6.25 km grid was presented [1]. It uses as input the full-resolution L1B radar cross-section product issued by the European Organisation for the Exploitation of Meteorological Satellites (EUMETSAT). This product contains the individual radar cross section values as produced by the on-board processor of the MetOp satellite carrying ASCAT. The spatial extent of the individual cross sections is limited by beam width in azimuth and by on-board processing in range. It is described by the spatial response function (SRF).

The radar cross section per beam attributed to a wind vector cell (WVC) is the average of all full-resolution radar cross sections with their centers falling within a circular aggregation area with radius $R_{\max}$. The same procedure is applied in processing of the well-known ASCAT-coastal product [2], which has an aggregation radius $R_{\max}$ of 15 km and a true spatial resolution of about 28 km. ASCAT-6.25 has an aggregation radius of 7.5 km and a true spatial resolution of about 17 km. Its wind quality is slightly worse though than that of ASCAT-coastal: it contains about $0.2\,\mathrm{m}^2/\mathrm{s}^2$ more noise variance in the wind components when compared with buoys and forecasts from the european centre for medium-range weather forecasts (ECMWF) in a triple collocation analysis [1]. Fig. 1 gives a schematic representation of the aggregation procedure, taken from [2].

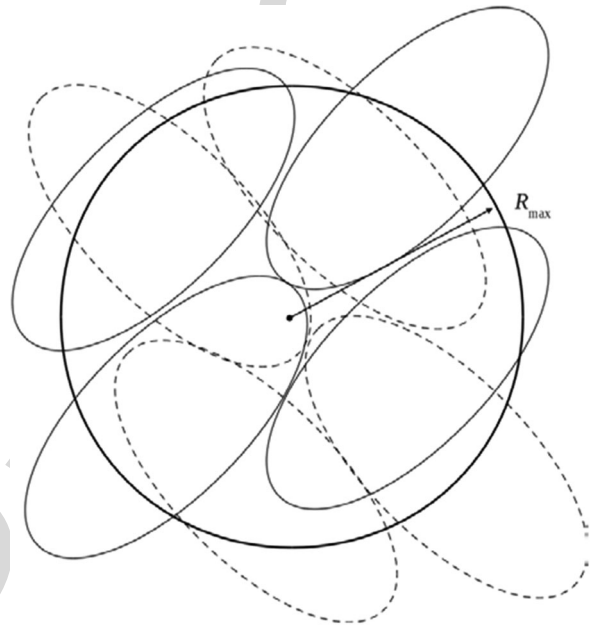

Fig. 1. Schematic illustration of scatterometer sampling for ASCAT-6.25 and ASCAT-coastal. A target WVC (thick solid line, with aggregation radius $R_{\max}$) is sampled from two different perspectives (for simplification), with measurement footprints indicated by solid and dashed ellipses, respectively.

The reason why ASCAT-6.25 is noisier than ASCAT-coastal is its smaller aggregation area. Less full-resolution radar cross sections contribute to the average radar cross section per beam, resulting in noisier backscatter and winds. This is in particular the case for the mid beam at low incidence angles. Furthermore, the individual full-resolution measurements are not evenly spread over the aggregation area. Therefore, the three beams may cover different parts of the ocean surface, leading to geophysical inconsistencies in the wind retrieval and lower quality winds. This will be important for dynamic mesoscale features—just the type of phenomena that requires high-resolution wind fields for analysis.

Fig. 2 shows the SRFs for single ASCAT full-resolution measurements for fore, mid, and aft beams (top, middle, and bottom panels, respectively), and for low, medium, and high incidence angles (left, middle, and right panels, respectively). As Fig. 2 pertains to measurements from the right beams in an ascending orbit close to the equator, the corresponding WVC numbers for ASCAT-coastal are 42, 62, and 82. The ASCAT-coastal WVC

Manuscript received June 30, 2016; revised September 16, 2016; accepted October 24, 2016. This work was supported by EUMETSAT as part of the Satellite Application Facility for Numerical Weather Prediction (NWP SAF). *(Corresponding author: Jur Vogelzang.)*

The authors are with the Royal Netherlands Meteorological Institute (KNMI), De Bilt, The Netherlands, 3731 GA (e-mail: Jur.Vogelzang@knmi.nl; Ad.Stoffelen@knmi.nl).

Color versions of one or more of the figures in this paper are available online at http://ieeexplore.ieee.org.

Digital Object Identifier 10.1109/JSTARS.2016.2623861

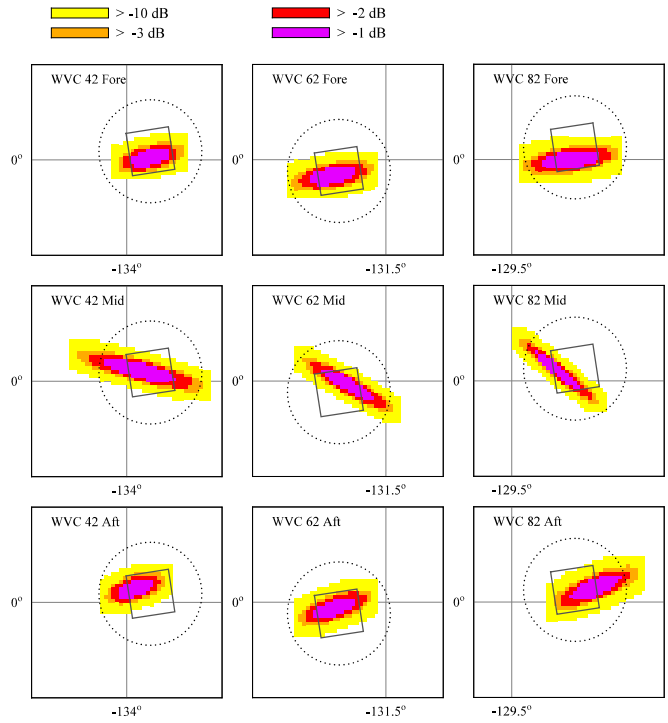

Fig. 2. Spatial response functions of a single ASCAT full-resolution radar cross-section measurement for the fore beam (top panels), mid beam (middle panels), and aft beam (bottom panels) for WVC's 42, 62, and 82 of the ASCAT-coastal product. The square box gives the WVC (size 12.5 km) and the dotted circle the boundary of the aggregation area (radius 15 km).

measuring 12.5 km by 12.5 km is indicated by the solid square, the aggregation area with 15 km radius is indicated by the doted circle. The magnitude of the SRF in dB is given by the colors.

The SRFs have an elliptical shape, and are to be compared to those in Fig. 1. The shape of the SRF's is determined by the antenna footprint, the range-gating, and the Doppler shift. The ellipses are quite elongated, notably for the mid beam. This is caused by on-board averaging of the antenna pulses: each full-resolution radar cross section is based on the running average of eight individual antenna pulses. The chirps for the fore and aft beams go in different directions (low to high frequency versus high to low), and Doppler shifts change the orientation of the ellipses in such a way that the fore and aft beam SRFs have almost the same orientation [3]. Fig. 2 also shows that the SRFs rapidly drop off to zero.

This study is a first attempt to improve on ASCAT-6.25 by exploiting the possibilities of the full-resolution L1B radar cross-section product. As noted in [1] improved radar sampling can be achieved by defining the WVC grid relative to the mid-beam measurement pattern. The average distance between two full-resolution measurements in the along-track direction is about 5.6 km, which restricts the WVC grid size to multiples of 5.6 km. Here, we concentrate on a WVC grid size of 5.6 km, referring to the wind products on this grid as ASCAT-5.6, and compare results with ASCAT-6.25.

Since the WVC grid is synchronized with the regular mid-beam measurements, it is not necessary to check for each individual WVC which measurement falls within the aggregation area, as is the procedure for the ASCAT-coastal and ASCAT-6.25 products. Instead, this search needs to be done only once for a single row of WVC's, and the results can be stored in a look-up table further referred to as aggregation table. However, the Metop orbit is slightly elliptical due to the nonspherical mass distribution of the Earth. This causes the orientation of the Metop platform to change periodically along its orbit, a phenomenon known in astronomy as libration. Due to libration, the beam samples may be shifted relatively to each other by as much as 60 km. This can be solved, at least partially, by a libration correction. The result is a very efficient aggregation algorithm. Moreover, the aggregation table may be edited manually to optimize the cumulative spatial response function (CSRF) of each beam separately and of all three beams together.

As in [1], the area within the -3 dB contour of the CSRF of all three beams is adopted as a measure for the true spatial resolution. Assuming the all-beams CSRF to have a circular contour, the diameter of that circle is considered as the true spatial resolution. We find that the spatial resolution is slightly worse for the ASCAT-5.6 products than that of ASCAT-6.25, but an ASCAT-5.6 product with manually edited aggregation table (to improve radar sampling) compares slightly better with buoys.

The paper is organized as follows. Section II contains a description of the data used in this study. The ASCAT-5.6 grid is defined in Section III. The aggregation table is introduced here, and the libration corrections are derived. Section IV contains the analysis of spatial resolution, beam overlap, and buoy comparison. The results are discussed in Section V. The paper ends with the conclusions in Section VI.

II. Data

In this study, we use the same data as in [1], but for the sake of completeness, their description is repeated here. The period of data comparison is August 2013.

We consider all full-resolution L1B ASCAT-A data from August 2013. The inversion scheme of the ASCAT Wind Data Processor (AWDP) is used [4], which provides up to four ambiguous solutions, called ambiguities, as well as their inversion residuals. In this study, the residual is not normalized to a maximum likelihood estimator and KNMI quality control (QC) is switched OFF. The 2DVAR ambiguity removal scheme is used to select the most probable solution from the ambiguities.

During processing, the scatterometer winds are collocated with forecasts from the ECMWF model as input for 2DVAR. The model winds, further referred to as background, are quadratically interpolated in time and bilinearly in space to the scatterometer winds. The background winds are used as initial guess for the ambiguity removal. It must be stressed here that the background fields are not in the highest resolution available, but on a grid size of about 70 km, as used in operational monitoring. This grid size is sufficient for the purposes of this study.

Buoy data were retrieved for August 2013 from the ECMWF MARS archive using all buoys not blacklisted. The buoy data are quality controlled and (where necessary) blacklisted by ECMWF [5]. The buoy winds are measured every hour by

averaging the wind speed and direction over 10 min. The real winds at a given anemometer height have been converted to 10 m equivalent neutral winds using the Liu, Katsaros, and Businger model [5], [6] in order to enable a good comparison with the 10 m scatterometer winds. The buoys passing QC are all moored buoys located in the Tropics (TOA, RAMA, and PIRATA buoys) and along the coast lines of North America and Europe. The minimum separation from the coast is about 15 km. The wind measurements are averaged over 10 min and issued once per hour. The buoy data were collocated with the scatterometer data with a maximum temporal separation of 30 min and a maximum spatial separation of the grid size divided by $\sqrt{2}$. In cases where more than one collocation was found for the same buoy at the same time, the collocation closest in position was selected.

One may argue that a temporal separation of 30 min may be too large for comparison with high-resolution scatterometer data. Moreover, buoy winds averaged over 10 min are representative for a scale of 4.2 km at 7 m/s, whereas the scatterometer products discussed here are the (almost) instantaneous average over an area of about 1000 km^2. Lin *et al.* [7] have shown that notably in the Tropics in convective situations wind variability is high, and that buoy measurements averaged over periods longer than 10 min are more representative for scatterometer winds. However, such an approach is considered outside the scope of this work.

III. WVC Grid Definition

The average distance between two full-resolution measurements in the along-track direction is about 5.6 km, which restricts the WVC grid size to multiples of 5.6 km. Here, we concentrate on a WVC grid size of 5.6 km and refer to the resulting wind product as ASCAT-5.6.

A. Handling of Missing Full-Resolution Data

The full-resolution radar cross-section data provided by EUMETSAT are ordered with antenna pulse time. The antennas are numbered one to six (left fore, left mid, left aft, right fore, right mid, and right aft, respectively). Each antenna at a time emits a pulse and receives its echo that is processed on-board. Also some averaging is done on-board, so a single radar cross-section value is the weighted average of eight antenna pulses [3].

The WVC grid is required to be free of gaps. The first problem encountered when defining a WVC grid synchronized with the ASCAT mid-beam measurements is that sometimes full-resolution data are missing. However, the number of missing antenna pulses can be determined with sufficient accuracy from the time between two pulses of the same antenna, which varies between 0.848 and 0.851 s with an average of about 0.84934 s for gap-free data.

B. Grid Definition and Aggregation Table

The definition of the WVC grid starts with the selection of an aggregation radius. For ASCAT-5.6, a value of 7.5 km is chosen to facilitate comparison with the ASCAT-6.25 product.

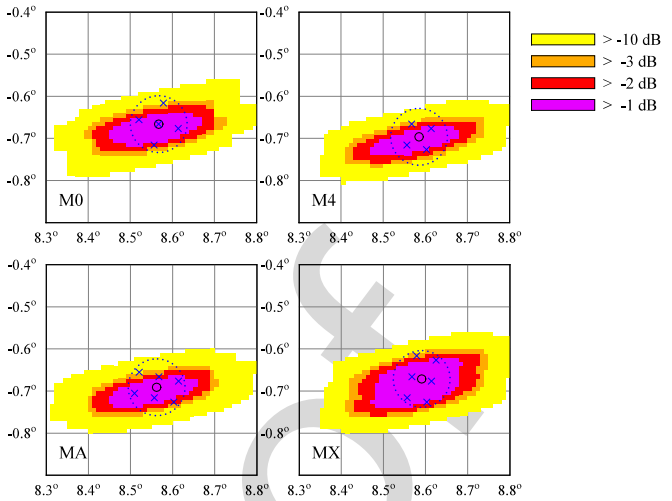

Fig. 3. Mid-beam aggregation patterns and CSRF for the four possible symmetrical ASCAT-5.6 grids at low incidence angle.

As noted above, radar sampling is poorest for the mid beam at low incidence angles. In order to maximize the number of mid-beam full-resolution measurements within the aggregation area, the WVC center must be located symmetrically with respect to them. For a mid-beam synchronized WVC grid, there are four possibilities, as shown in Fig. 3, for an example at lowest incidence angle near the equator: WVC center coinciding with a measurement center (M0, upper left), WVC center in between four measurements (M4, upper right), WVC center between two neighboring measurements in the along-track direction (MA, lower left), and WVC center between two measurements in the cross-track direction (MX, lower right). The full-resolution measurement centers are indicated as crosses in Fig. 3, the WVC center as a small solid circle, and the 7.5 km aggregation area as a larger dotted circle. In color are the values of the CSRF. It is the sum of the SRFs of all contributing measurements, normalized to a maximum value of 1 (0 dB). The SRF's were computed following the approach in [3].

Fig. 3 shows that the MA and MX grids are to be preferred since they contain six measurements in the aggregation area whereas M0 has five and M4 only four. The CSRF for the MX grid has the most circular shape, so this grid is selected.

Next, a row of WVC's with 5.6 km grid size is defined in the mid-beam (cross-track) direction at each side of the satellite track, starting from a particular row of mid-beam full-resolution data. If the distance between the WVC's is kept fixed, the measurement pattern will soon become less optimal, since the measurements are unevenly spaced in the mid-beam direction. Therefore, the MX choice is kept for each WVC, so all WVC centers are located between two neighboring measurements in the cross-track direction. The consequence is that the distance between neighboring WVC's in the cross-track direction is no longer constant.

Finally, the measurements contributing to each WVC in one row are found. Their relative along- and cross-track indices are stored in a look-up table named aggregation table. When deriving ocean surface winds from the radar cross sections, it suffices

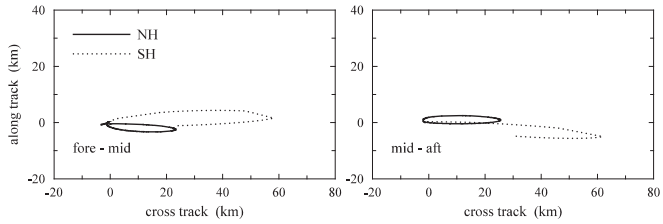

Fig. 4. Libration in along-track versus cross-track distances between fore and mid-beam centers (left-hand panel) and between mid and aft beam centers (right-hand panel). The gap in the Southern Hemisphere (SH) curves (dotted curves) is caused by land overpass.

to read in the full-resolution data and the appropriate aggregation table. The full-resolution cross sections contributing to a particular WVC area are then easily found from the aggregation table. This constitutes a much more efficient algorithm than searching through the full-resolution data for each WVC as implemented in AWDP for ASCAT-coastal and ASCAT-6.25. This is important, since ASCAT-5.6 may have 200 WVC's in a row and over 7100 rows in an orbit.

C. Libration Correction

There is, however, a complication in applying aggregation tables. In order to keep its antennas pointed to the Earth's surface, the Metop platform has to rotate once every orbit around its axis perpendicular to the orbital plane. This rotation has constant angular velocity, but the orbit is slightly elliptical due to the nonuniform mass distribution of the Earth. As a result, the orientation of the Metop platform as viewed from the Earth changes slightly during its orbit, a movement known in astronomy as libration. Fig. 4 shows the along-track and cross-track distances between the left fore and left mid beam (left-hand panel) and between the left mid and left aft beam (right-hand panel), for the lowest incidence angle during one orbit on August 1, 2013. The solid curves pertain to the Northern Hemisphere, the dotted ones to the Southern Hemisphere. The gap in the dotted curves is caused by land overpass. Above the equator—where the aggregation tables were generated—the beams overlap, but over the poles, notably the South Pole, the distance between the beams increases to 60 km.

This can be corrected for by calculating WVC-dependent offsets in the aggregation table for the fore and aft beams, such that these beams overlap as much as possible with the mid beam. Let the central position of each beam in a WVC be defined as the average geographical latitude and longitude of the full-resolution measurements contributing to the radar cross section attributed to that WVC. First consider the fore beam.

Let Δ_A^f be the distance between the measurements in the along-track direction ($\Delta_A^f \approx 5.6$ km) and Δ_R^f that in the range direction. The positive range direction is outward from the satellite. It makes an angle of $\pm 45^\circ$ with the along-track direction, so the projection of Δ_R^f in the cross-track direction is $\delta_X^f = \frac{1}{2}\sqrt{2}\Delta_R^f$ and that in the along-track direction is $\delta_A^f = \frac{1}{2}\sqrt{2}\Delta_R^f$. Fig. 3 shows a schematic representation for the right fore beam. Let d_A^f and d_X^f be the distance between the central positions of fore- and mid beam in the along-track and cross-track directions, respectively. The offsets m_A^f and m_R^f needed to shift the fore beam as close as possible to the mid beam satisfy

$$d_A^f = m_A^f \Delta_A^f + m_R^f \delta_A^f = m^f{}_A \Delta^f{}_A + \tfrac{1}{2}\sqrt{2} m_R^f \Delta_R^f, \quad (1a)$$

$$d_X^f = m_R^f \delta_X^f = \tfrac{1}{2}\sqrt{2} m_R^f \Delta_R^f. \quad (1b)$$

From (1a) and (1b), it immediately follows that

$$m_A^f = \frac{d_A^f - d_X^f}{\Delta_A^f}, \quad m_R^f = \sqrt{2}\frac{d_X^f}{\Delta_R^f}. \quad (2)$$

The aft beam makes an angle of $\pm 135^\circ$ with the along-track direction, so analogous to the above, the projections of Δ_R^a on the cross-track and along-track directions are $\delta_X^a = \frac{1}{2}\sqrt{2}\Delta_R^a$ and $\delta_A^a = -\frac{1}{2}\sqrt{2}\Delta_R^a$. Now the offsets m_A^a and m_R^a must satisfy

$$d_A^a = m_A^a \Delta_A^a + m_R^a \delta_A^a = m_A^a \Delta_A^a - \tfrac{1}{2}\sqrt{2} m_R^a \Delta_R^a, \quad (3a)$$

$$d_X^a = m_R^a \delta_X^a = \tfrac{1}{2}\sqrt{2} m_R^a \Delta_R^a. \quad (3b)$$

This is solved as

$$m_A^a = \frac{d_A^a + d_X^a}{\Delta_A^a}, \quad m_R^a = \sqrt{2}\frac{d_X^a}{\Delta_R^a}. \quad (4)$$

Of course the offsets are integers, so the expressions in the right-hand sides of (2) and (4) are rounded off to the nearest integer. The procedure must be iterated because the along-track and cross-track measurement distances Δ_A and Δ_R are not constant over the swath, notably Δ_R at low incidence. This iteration converges in a few steps and does not add much to the processing time.

D. Manual Editing of the Aggregation Table

The libration correction must be done for every WVC. Therefore, the aggregation table does not need to be very precise, as any mismatch between the beams will be compensated for as good as possible. As a consequence, the aggregation table can be edited manually for, say, the left fore and left mid beam, and defined for the other beams symmetrically with respect to the along-track and cross-track directions.

E. Grids Used

In this paper, two ASCAT-5.6 products will be studied. The first product is obtained by using an aggregation table constructed for one row of WVC's and for each beam separately by aggregating the measurements in a circular aggregation area with 7.5 km radius. This is equivalent to ASCAT-6.25 sampling, except that the same aggregation table is used for all rows of WVC's, resulting in more uniform radar sampling. This product will be further referred to as (ordinary) ASCAT-5.6.

The second product is obtained by manually adding measurements to the aggregation table in such a way that the -3 dB contours of the resulting CSRF's for the left fore and left mid-beam cover as good as possible the aggregation area with radius 7.5 km. For the left fore beam there are two patterns, one for WVC's 1 to 65 and one for WVC's 66 to 100. For the

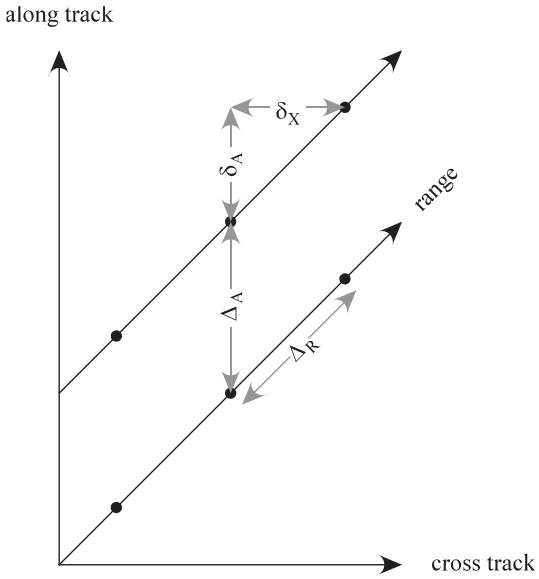

Fig. 5. Geometry for libration correction of the right fore beam. The solid dots indicate the footprint centers of the right fore beam.

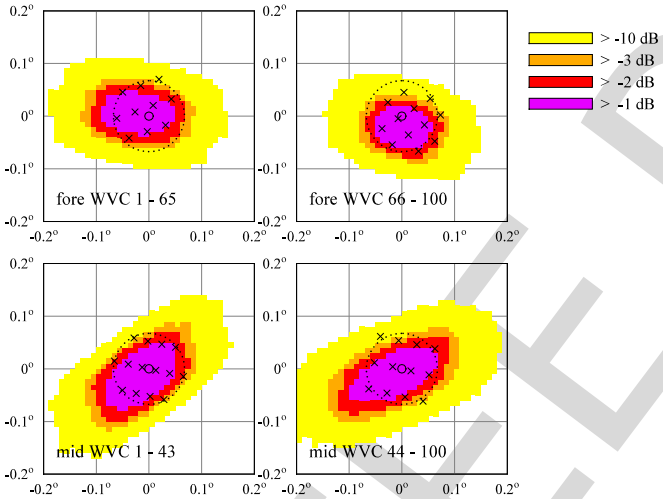

Fig. 6. Aggregation patterns for the improved ASCAT-5.6 product.?>

left mid beam there are also two patterns, one for WVC's 1 to 43 and one for WVC's 44 to 100. Fig. 6 shows the aggregation patterns used for the left fore and left mid beams. The contributing measurements are indicated by crosses, the WVC center by the small solid circle, and the edge of the aggregation area with 7.5 km radius by the dotted circle. The CSRFs in Fig. 6 are for WVCs 32 (upper left panel), 84 (upper right panel), 22 (lower left panel), and 72 (lower right panel), halfway in the range of validity of the aggregation pattern. The aggregation table for the other beams is defined symmetrically with respect to the along-track and cross-track directions. This product will be referred to as improved ASCAT-5.6.

From Fig. 6, it is clear that it is not easy to define circular CSRFs, because of the elongated elliptical shape of the SRFs (see also Fig. 2). Comparison of Fig. 6 with Fig. 3 shows that the improved product has twice as many contributing

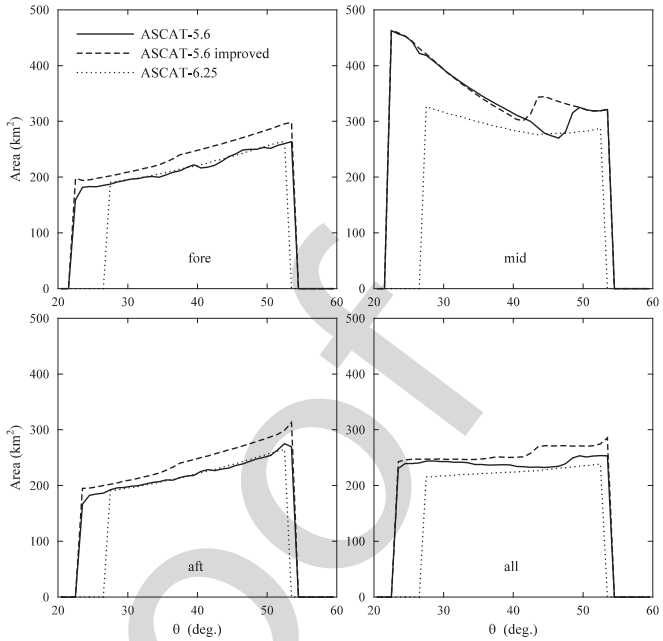

Fig. 7. Area covered by the −3 dB contour of the CSRF versus incidence angle.

measurements in the mid beam at low incidence than the ordinary ASCAT-5.6 product.

IV. Results

A. Spatial Resolution and Overlap

Fig. 7 shows the area covered within the −3 dB contour of the CSRF for the two products defined in the previous section and for ASCAT-6.25 as a function of incidence angle. The results in Fig. 5 are based on data from one orbit on August 16, 2013. The improved ASCAT-5.6 product has the largest area, notably in the mid beam at small incidence angle. This is as expected, because the improved grid was defined to have as much SRFs as possible contributing to a WVC. The ordinary ASCAT-5.6 product has larger area than the ASCAT-6.25 product in the mid beam, but not in the fore and aft beams. This is because ASCAT-5.6 uses the same optimal aggregation pattern for the mid beam, so the number of contributing mid-beam SRFs is constant for each WVC. For ASCAT-6.25, this number varies along the swath, and also less mid-beam SRFs may contribute to a WVC, leading to a −3 dB CSRF area that is smaller than that of ASCAT-5.6. For the fore and aft beams, sampling is less critical, so the differences between the three products are smaller.

The mid-beam area decreases with increasing the incidence angle, while the fore and aft beam areas increase. As a result, the −3 dB CSRF area for all beams (lower right panel of Fig. 7) varies little with incidence angle. Assuming the −3 dB contour of the all-beams CSRF area to be circular, the diameter of this circle is 19 km for the improved ASCAT-5.6 product, 18 km for the ordinary ASCAT-5.6 product, and 17 km for the ASCAT-6.25 product. These values are adopted as measures of the true spatial resolution.

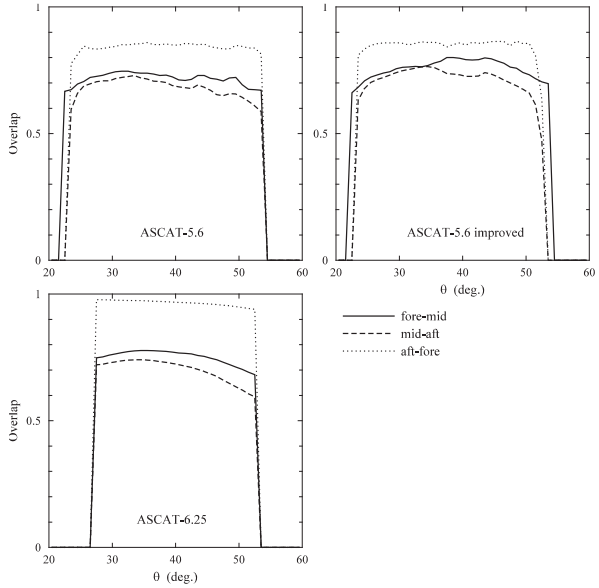

Fig. 8. Overlaps between the three beam pairs as a function of incidence angle.

Despite the fact that the two ASCAT-5.6 products have larger CSRFs per beam, their overall true spatial resolution is almost the same as that of ASCAT-6.25. This is caused by the fact that each of the three beams illuminates a slightly different area. As a result, the all beam CSRF has a narrow peak, yielding good spatial resolution, but also a long tail, enhancing geophysical errors. This can be understood from the beam overlap. The overlap $O_{\alpha\beta}$ between beams α and β is defined as in [1]

$$O_{\alpha\beta} = \frac{I_{\alpha\beta}^2}{I_{\alpha\alpha} I_{\beta\beta}} \tag{5}$$

with

$$I_{\alpha\beta} = \int\int d\lambda d\varphi \, \cos\varphi \, C_\alpha(\lambda,\varphi) \, C_\beta(\lambda,\varphi) \tag{6}$$

where C_α stands for the CSRF of beam α as a function of geographical longitude λ and latitude φ, and the integration is over the entire domain of the CSRFs.

Fig. 8 shows the overlap between the three beam pairs for the two ASCAT-5.6 products and ASCAT-6.25 as a function of incidence angle. Fig. 8 is based on data from the same orbit as used for Fig. 7. The overlap between the fore and aft beam of the ordinary and improved ASCAT-5.6 products is worse than that of ASCAT-6.25. This is due to the fact that the libration correction is discrete, so it is unable to shift the fore and aft beam centers exactly on the mid-beam center. On the other hand, the improved ASCAT-5.6 has slightly better overlap between fore and mid beam and between mid and aft beam than ASCAT-6.25. This is because the mid-beam CSRF is better defined.

B. Buoy Comparison

The ASCAT winds were collocated with buoys. Table I shows the standard deviation of the difference between scatterometer and buoys for wind speed, wind direction, zonal wind component u, and meridional wind component v. Only collocations common to all three datasets were considered, resulting in 2475 collocations. Wind direction statistics were only considered in case all wind speeds exceeded 4 m/s, resulting in 1712 collocations. The accuracies in the bottom row are based on the inverse square root of the number of collocations.

TABLE I
BUOY COMPARISON

Product	σ_s (m/s)	σ_d (deg)	σ_u (m/s)	σ_v (m/s)
ASCAT-6.25	0.99	17.3	1.48	1.61
ASCAT-5.6	1.00	17.3	1.46	1.65
ASCAT-5.6 Improved	0.99	16.8	1.45	1.61
Accuracy	0.02	0.4	0.03	0.03

Table I shows that there is little difference between ASCAT-6.25 and ASCAT-5.6, though the agreement for u is slightly better and that for v is slightly worse. The improved ASCAT-5.6 product compares best with buoys, in particular for the wind direction. This indicates that manual editing of the aggregation tables for the left-fore and left-mid beam and symmetric definition of the other beams indeed leads to a better product. In particular, the doubling of the number of contributing measurements in the mid beam at low incidence angles leads to less noise in the radar cross sections, and hence better wind retrievals.

Nevertheless, Table I shows that the differences are on the edge of being significant, and more work on much larger datasets remains to be done in order to reduce statistical uncertainty.

C. Some Examples

Fig. 9 shows improved ASCAT-5.6 (upper panel) and ASCAT-6.25 (lower panel) wind fields of a frontal zone south of Australia recorded by ASCAT-A on July 31, 2013 (orbit starting at 22:42 UTC). Blue arrows denote valid winds and purple arrows winds flagged by the variational QC. The latter control flag is set when the mismatch between scatterometer observation and background wind field exceeds a certain limit. This is often caused by mispositioning of mesoscale wind structures in the background. Fig. 9 shows some ambiguity removal errors in the frontal zone as encircled arrows. The ASCAT-6.25 scene contains 11 clear ambiguity removal errors; the improved ASCAT-5.6 scene 9, despite its higher density of retrieved winds. Though there may be discussion on the exact number of ambiguity removal errors—only the most obvious ones were marked in Fig. 7—the improved ASCAT-5.6 product contains less errors than the ASCAT-6.25 product. In particular, the two ambiguity removal errors in the ASCAT-6.25 product near the 138° meridian have disappeared in the improved ASCAT-5.6 product. Note also that all ambiguity removal errors in the scene are flagged in the improved ASCAT-5.6 product, but not in the ASCAT-6.25 product.

Another example is given by Fig. 10, which shows a convective area in the Tropical western Pacific recorded by ASCAT-A

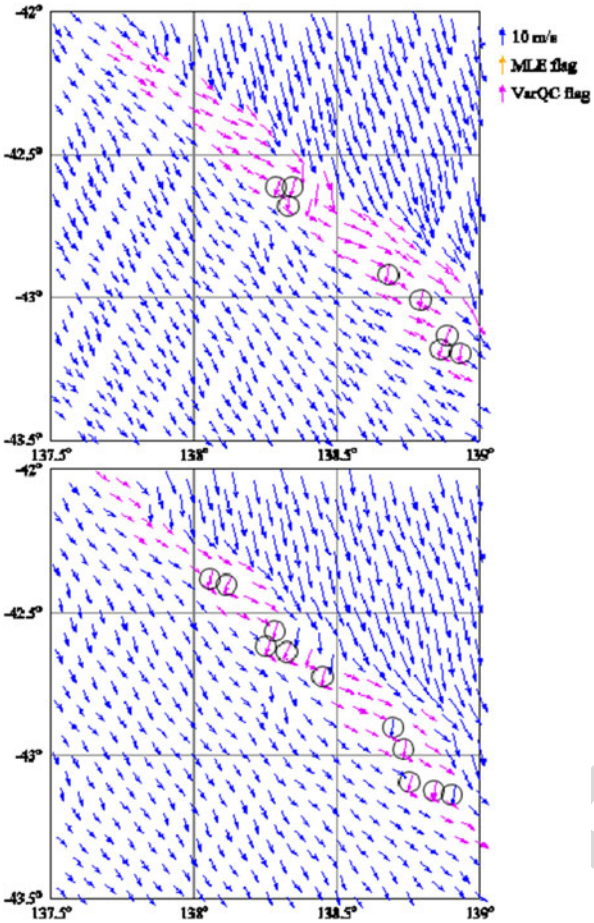

Fig. 9. Improved ASCAT-5.6 (upper panel) and ASCAT-6.25 (lower panel) wind fields over a frontal zone south of Australia recorded July 31, 2013. Wind vectors with obvious ambiguity removal errors have been encircled.

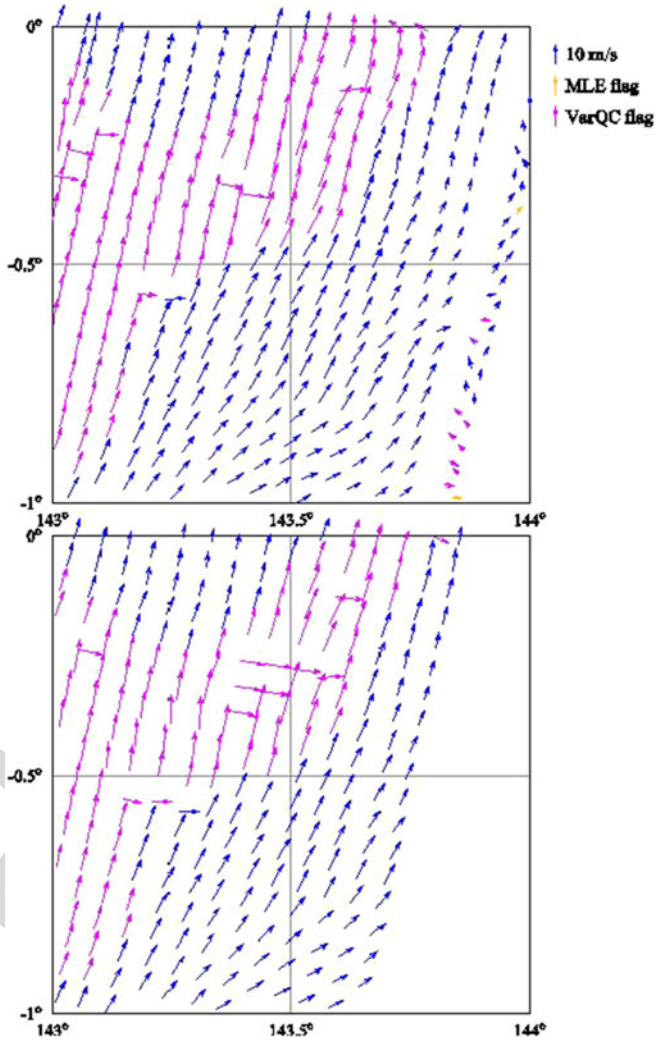

Fig. 10. Improved ASCAT-5.6 (upper panel) and ASCAT-6.25 (lower panel) wind fields over a convective area in the Tropical western Pacific recorded August 2, 2013.

on August 2, 2013 shortly after 0:00. The flow is from South to North, but ambiguity removal errors cause some wind vectors to point to the West. These are easy to recognize, so they have not been marked. The top panel, showing improved ASCAT-5.6 data, contains 8 ambiguity removal errors, while the bottom panel, showing ASCAT-6.25, contains 13. As in Fig. 9, the variational QC flag is set in a number of WVCs (purple arrows), caused by poor representation of the convective mesoscale structure in the ECMWF background wind field.

Note that the improved ASCAT-5.6 scene in Fig. 10 covers a larger area than the ASCAT-6.25 scene, because it has extra WVCs at the Eastern side of the swath, where the incidence angle is highest. This is because ASCAT-5.6 processing accepts measurements at higher incidence angles than ASCAT-6.25 processing. The quality of these additional retrievals is poor, so an operational product should better not contain them, either by limiting the incidence angle range or by improving QC.

V. Discussion

The results in Section IV show that it is indeed possible to define an ASCAT wind product on a 5.6 km grid synchronized with the ASCAT mid-beam pattern with better quality than the ASCAT-6.25 product, though at the cost of a slightly reduced true spatial resolution (19 km against 17 km) and irregular grid size.

However, the possibilities for defining the WVC grid and the aggregation pattern are far from exhausted. The MX grid in Fig. 3 leads to a more circular CSRF than the MA grid, but the MA grid has a more compact CSRF. Manual editing of the MA aggregation table may lead to better results.

In the products, presented in this study, it was attempted to retain a rectangular WVC grid with the same size in along-track and cross-track directions as much as possible. The requirement that the mid-beam center should fall exactly between two measurements in the cross-track directions leads to nonuniform grid sizes in the cross-track direction, see Figs. 9 and 10. Another possibility is to synchronize the grid in the cross-track direction also with the mid-beam measurement pattern. One may select a suitable aggregation pattern for the left fore and left mid beams, define those for the other beams symmetrically with respect to the along-track and cross-track directions, and apply the

aggregation pattern every *n*th measurement in the range direction. This will lead to a product with constant radar sampling characteristics, but different grid sizes in along-track and cross-track directions. Moreover, the grid size in the cross-track direction will vary with the incidence angle: it will be larger at small incidence and smaller at large incidence. The same holds for the true spatial resolution. Such a product will be more comfortable to the eye than the improved ASCAT-5.6 products shown in Figs. 9 and 10. More investigations are needed to assess the quality of such products, and extensive interactions with potential end users are required to arrive at products that suit their needs.

The elliptical shape of the individual SRFs (see Fig. 2) poses a lower limit on the true spatial resolution that can be obtained, in particular at low incidence angles. The possibility to define a wind product with optimized true spatial resolution at intermediate and high incidence, at the cost of noisier winds, also remains to be investigated.

In this study, the high-resolution wind products were compared with buoy winds averaged over 10 min. As has been shown in [7], it is better to compare with buoy winds averaged over a longer time period that is centered around the scatterometer measurement time. At 7 m/s wind speed, buoy measurements over 10 min are representative for a scale of about 4 km, which is much smaller than the area covered by a scatterometer WVC. This is also a subject for further research.

A final remark pertains the successors of the present series of ASCAT instruments that will be mounted on the second generation of polar-orbiting Metop satellites (Metop-SG) from 2022 onwards. These will have no on-board averaging, resulting in a denser measurement pattern and SRFs with a more circular shape, offering even more possibilities to define ultrahigh-resolution wind products.

VI. Conclusion

In this study, two new high-resolution ASCAT wind products on a 5.6 km grid were compared to the ASCAT-6.25 product. The ASCAT-5.6 grid is synchronized to the ASCAT mid-beam measurements, and the cross-track grid position is determined by the requirement that it should fall exactly between two consecutive measurements. This leads to nonuniform grid sizes in the cross-track direction. A very efficient processing scheme is arrived at by using aggregation tables in combination with a libration correction.

The ordinary ASCAT-5.6 product is similar to the ASCAT-6.25 product, but with constant radar sampling. The improved ASCAT-5.6 product employs an aggregation table that has been edited manually to maximize the number of contributing measurements.

The true spatial resolution is defined as the diagonal of the -3 dB contour of the all-beams CSRF. For the ASCAT-6.25, ASCAT-5.6, and improved ASCAT-5.6 products it is 17, 18, and 19 km, respectively. The ASCAT-5.6 products have poorer overlap between the beams than the ASCAT-6.25 product, because the libration correction is discrete. The improved ASCAT-5.6 product compares better with buoys than the other two products, because the increased number of measurements contributing to a WVC leads to better quality winds. This is confirmed by a few examples showing less ambiguity removal errors in the improved ASCAT -5.6 product than in the ASCAT-6.25 product. It is concluded that the improved ASCAT-5.6 product has better quality than the ASCAT-6.25 product, at the cost of a slightly inferior true spatial resolution.

No QC of the inversion was considered here, but generally a more consistent retrieval also provides a more consistent QC. This needs verification in future work.

The ASCAT-5.6 wind products presented in this study are the first to exploit the possibilities offered by the full-resolution product. A number of options remains to be investigated, and extensive interaction with end users will be required to arrive at wind products that suit their needs.

References

[1] J. Vogelzang, A. Stoffelen, R. Lindsley, A. Verhoef, and J. Verspeek, "The ASCAT-6.25-km product," *IEEE J. Sel. Topics Remote Sens.*, 2016, doi: 10.1109/JSTARS.2016.2623862

[2] A. Verhoef, M. Portabella, and A. Stoffelen, "High-resolution ASCAT scatterometer winds near the coast," *IEEE Trans. Geosci. Remote Sens.*, vol. 50, no. 7, pp. 2481–2487, Jul. 2012, doi:10.1109/TGRS.2016.2544835

[3] R. D. Lindsley, C. Anderson, J. Figa-Saldaña, and D. Long, "A parameterized ASCAT measurement spatial response function," *IEEE Trans. Geosci. Remote Sens.*, vol. 54, no. 8, pp. 4570–4579, Aug. 2016. doi:10.1109/TGRS.2016.2544835

[4] *ASCAT* Wind Product User Manual, KNMI, De Bit, The Netherlands, 2013. [Online]. Available: http://projects.knmi.nl/ scatterometer/publications/pdf/ASCAT_Product_Manual.pdf

[5] J. Bidlot, D. Holmes, P. Wittmann, R. Lalbeharry, and H. Chen, "Intercomparison of the performance of operational ocean wave forecasting systems with buoy data," *Weather Forecasting*, vol. 17, pp. 287–310, 2002, doi:10.1175/1520-0434(2002)017<0287:IOTPOO>2.0.CO;2

[6] W. T. Liu, K. B. Katsaros, and J. A. Businger, "Bulk parameterization of air-sea exchanges of heat and water vapor including the molecular constraints in the interface," *J. Atmos. Sci.*, vol. 36, pp. 1722–1735, 1979, doi:10.1175/1520-0469(1979)036<1722:BPOASE>2.0.CO;2

[7] W. Lin, M. Portabella, A. Stoffelen, A. Verhoef, and A. Turiel, "ASCAT wind quality control near rain," *IEEE Trans. Geosci. Remote Sens.*, vol. 53, no. 8, pp. 4165–4177, Aug. 2015.

Jur Vogelzang was born in The Netherlands in 1955. He received the M.Sc. degree in theoretical physics from the Free University, Amsterdam, The Netherlands, in 1981, and the Ph.D. degree in physics on radar remote sensing from the University of Utrecht, Utrecht, The Netherlands, in 1998.

He is currently with the Royal Netherlands Meteorological Institute (KNMI), De Bilt, The Netherlands, where he is working on scatterometer wind products.

Ad Stoffelen was born in 1962 in The Netherlands. He received the M.Sc. degree in physics from the Technical University of Eindhoven, Eindhoven, The Netherlands, in 1987, and the Ph.D. degree in meteorology on scatterometry from the University of Utrecht, Utrecht, The Netherlands.

He currently leads a group on active satellite sensing at KNMI and is involved in topics from future missions and retrieval to 24/7 operations, user training and services. He is also deeply involved in the European Space Agency ADM-Aeolus Doppler Wind Lidar mission.

ASCAT Ultrahigh-Resolution Wind Products on Optimized Grids

Jur Vogelzang and Ad Stoffelen

***Abstract*—The accuracy and spatial resolution of ultrahigh-resolution wind products derived from full-resolution ASCAT radar cross-section measurements are determined by the size and shape of the aggregation area. Current high-resolution products (ASCAT-coastal and ASCAT-6.25) are defined on a regular swath grid (size 12.5 and 6.25 km, respectively) and use a circular aggregation area (15 and 7.5 km radius resp.). For ASCAT-6.25, such approach leads to poor radar sampling, causing noise in the retrieved winds, and poor beam overlap, causing geophysical errors. More regular radar sampling and improved beam overlap can be obtained by using a grid that is synchronized with respect to the ASCAT mid-beam full-resolution measurements. This results in a new generation of ASCAT wind products. It is shown that a product on a 5.6 km grid size (on average) with optimized radar sampling compares better to buoys than ASCAT-6.25, but at the cost of an irregular grid and slightly degraded spatial resolution.**

***Index Terms*—Radar, wind.**

I. Introduction

STUDIES of dynamic mesoscale features over the ocean like convective cells, coastal jets, and von Kármán vortices in the wake of isles, require high-resolution wind data. Spaceborne scatterometers can provide such information. Recently, the ASCAT-6.25 product which contains ocean surface vector winds on a 6.25 km grid was presented [1]. It uses as input the full-resolution L1B radar cross-section product issued by the European Organisation for the Exploitation of Meteorological Satellites (EUMETSAT). This product contains the individual radar cross section values as produced by the on-board processor of the MetOp satellite carrying ASCAT. The spatial extent of the individual cross sections is limited by beam width in azimuth and by on-board processing in range. It is described by the spatial response function (SRF).

The radar cross section per beam attributed to a wind vector cell (WVC) is the average of all full-resolution radar cross sections with their centers falling within a circular aggregation area with radius $R_{\max}$. The same procedure is applied in processing of the well-known ASCAT-coastal product [2], which has an aggregation radius $R_{\max}$ of 15 km and a true spatial resolution of about 28 km. ASCAT-6.25 has an aggregation radius of 7.5 km and a true spatial resolution of about 17 km. Its wind quality is slightly worse though than that of ASCAT-coastal: it contains about $0.2\,\mathrm{m}^2/\mathrm{s}^2$ more noise variance in the wind components when compared with buoys and forecasts from the european centre for medium-range weather forecasts (ECMWF) in a triple collocation analysis [1]. Fig. 1 gives a schematic representation of the aggregation procedure, taken from [2].

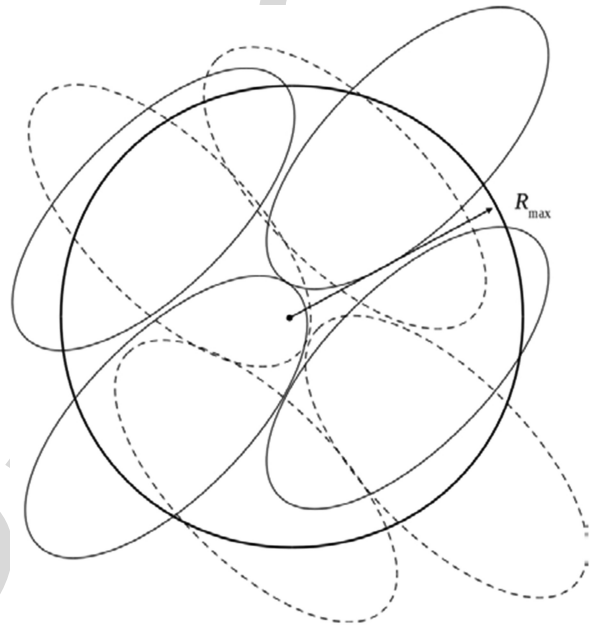

Fig. 1. Schematic illustration of scatterometer sampling for ASCAT-6.25 and ASCAT-coastal. A target WVC (thick solid line, with aggregation radius $R_{\max}$) is sampled from two different perspectives (for simplification), with measurement footprints indicated by solid and dashed ellipses, respectively.

The reason why ASCAT-6.25 is noisier than ASCAT-coastal is its smaller aggregation area. Less full-resolution radar cross sections contribute to the average radar cross section per beam, resulting in noisier backscatter and winds. This is in particular the case for the mid beam at low incidence angles. Furthermore, the individual full-resolution measurements are not evenly spread over the aggregation area. Therefore, the three beams may cover different parts of the ocean surface, leading to geophysical inconsistencies in the wind retrieval and lower quality winds. This will be important for dynamic mesoscale features—just the type of phenomena that requires high-resolution wind fields for analysis.

Fig. 2 shows the SRFs for single ASCAT full-resolution measurements for fore, mid, and aft beams (top, middle, and bottom panels, respectively), and for low, medium, and high incidence angles (left, middle, and right panels, respectively). As Fig. 2 pertains to measurements from the right beams in an ascending orbit close to the equator, the corresponding WVC numbers for ASCAT-coastal are 42, 62, and 82. The ASCAT-coastal WVC

Manuscript received June 30, 2016; revised September 16, 2016; accepted October 24, 2016. This work was supported by EUMETSAT as part of the Satellite Application Facility for Numerical Weather Prediction (NWP SAF). *(Corresponding author: Jur Vogelzang.)*

The authors are with the Royal Netherlands Meteorological Institute (KNMI), De Bilt, The Netherlands, 3731 GA (e-mail: Jur.Vogelzang@knmi.nl; Ad.Stoffelen@knmi.nl).

Color versions of one or more of the figures in this paper are available online at http://ieeexplore.ieee.org.

Digital Object Identifier 10.1109/JSTARS.2016.2623861

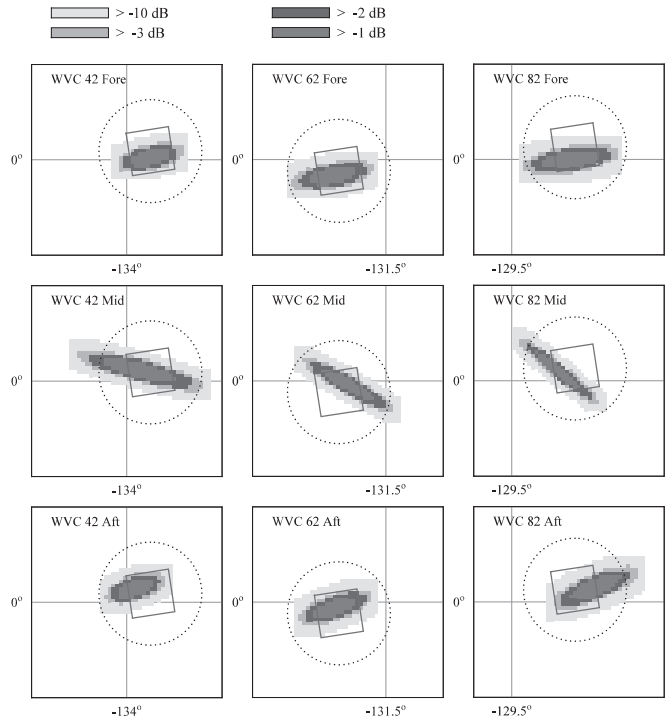

Fig. 2. Spatial response functions of a single ASCAT full-resolution radar cross-section measurement for the fore beam (top panels), mid beam (middle panels), and aft beam (bottom panels) for WVC's 42, 62, and 82 of the ASCAT-coastal product. The square box gives the WVC (size 12.5 km) and the dotted circle the boundary of the aggregation area (radius 15 km).

measuring 12.5 km by 12.5 km is indicated by the solid square, the aggregation area with 15 km radius is indicated by the doted circle. The magnitude of the SRF in dB is given by the colors.

The SRFs have an elliptical shape, and are to be compared to those in Fig. 1. The shape of the SRF's is determined by the antenna footprint, the range-gating, and the Doppler shift. The ellipses are quite elongated, notably for the mid beam. This is caused by on-board averaging of the antenna pulses: each full-resolution radar cross section is based on the running average of eight individual antenna pulses. The chirps for the fore and aft beams go in different directions (low to high frequency versus high to low), and Doppler shifts change the orientation of the ellipses in such a way that the fore and aft beam SRFs have almost the same orientation [3]. Fig. 2 also shows that the SRFs rapidly drop off to zero.

This study is a first attempt to improve on ASCAT-6.25 by exploiting the possibilities of the full-resolution L1B radar cross-section product. As noted in [1] improved radar sampling can be achieved by defining the WVC grid relative to the mid-beam measurement pattern. The average distance between two full-resolution measurements in the along-track direction is about 5.6 km, which restricts the WVC grid size to multiples of 5.6 km. Here, we concentrate on a WVC grid size of 5.6 km, referring to the wind products on this grid as ASCAT-5.6, and compare results with ASCAT-6.25.

Since the WVC grid is synchronized with the regular mid-beam measurements, it is not necessary to check for each individual WVC which measurement falls within the aggregation area, as is the procedure for the ASCAT-coastal and ASCAT-6.25 products. Instead, this search needs to be done only once for a single row of WVC's, and the results can be stored in a look-up table further referred to as aggregation table. However, the Metop orbit is slightly elliptical due to the nonspherical mass distribution of the Earth. This causes the orientation of the Metop platform to change periodically along its orbit, a phenomenon known in astronomy as libration. Due to libration, the beam samples may be shifted relatively to each other by as much as 60 km. This can be solved, at least partially, by a libration correction. The result is a very efficient aggregation algorithm. Moreover, the aggregation table may be edited manually to optimize the cumulative spatial response function (CSRF) of each beam separately and of all three beams together.

As in [1], the area within the -3 dB contour of the CSRF of all three beams is adopted as a measure for the true spatial resolution. Assuming the all-beams CSRF to have a circular contour, the diameter of that circle is considered as the true spatial resolution. We find that the spatial resolution is slightly worse for the ASCAT-5.6 products than that of ASCAT-6.25, but an ASCAT-5.6 product with manually edited aggregation table (to improve radar sampling) compares slightly better with buoys.

The paper is organized as follows. Section II contains a description of the data used in this study. The ASCAT-5.6 grid is defined in Section III. The aggregation table is introduced here, and the libration corrections are derived. Section IV contains the analysis of spatial resolution, beam overlap, and buoy comparison. The results are discussed in Section V. The paper ends with the conclusions in Section VI.

II. Data

In this study, we use the same data as in [1], but for the sake of completeness, their description is repeated here. The period of data comparison is August 2013.

We consider all full-resolution L1B ASCAT-A data from August 2013. The inversion scheme of the ASCAT Wind Data Processor (AWDP) is used [4], which provides up to four ambiguous solutions, called ambiguities, as well as their inversion residuals. In this study, the residual is not normalized to a maximum likelihood estimator and KNMI quality control (QC) is switched OFF. The 2DVAR ambiguity removal scheme is used to select the most probable solution from the ambiguities.

During processing, the scatterometer winds are collocated with forecasts from the ECMWF model as input for 2DVAR. The model winds, further referred to as background, are quadratically interpolated in time and bilinearly in space to the scatterometer winds. The background winds are used as initial guess for the ambiguity removal. It must be stressed here that the background fields are not in the highest resolution available, but on a grid size of about 70 km, as used in operational monitoring. This grid size is sufficient for the purposes of this study.

Buoy data were retrieved for August 2013 from the ECMWF MARS archive using all buoys not blacklisted. The buoy data are quality controlled and (where necessary) blacklisted by ECMWF [5]. The buoy winds are measured every hour by

averaging the wind speed and direction over 10 min. The real winds at a given anemometer height have been converted to 10 m equivalent neutral winds using the Liu, Katsaros, and Businger model [5], [6] in order to enable a good comparison with the 10 m scatterometer winds. The buoys passing QC are all moored buoys located in the Tropics (TOA, RAMA, and PIRATA buoys) and along the coast lines of North America and Europe. The minimum separation from the coast is about 15 km. The wind measurements are averaged over 10 min and issued once per hour. The buoy data were collocated with the scatterometer data with a maximum temporal separation of 30 min and a maximum spatial separation of the grid size divided by $\sqrt{2}$. In cases where more than one collocation was found for the same buoy at the same time, the collocation closest in position was selected.

One may argue that a temporal separation of 30 min may be too large for comparison with high-resolution scatterometer data. Moreover, buoy winds averaged over 10 min are representative for a scale of 4.2 km at 7 m/s, whereas the scatterometer products discussed here are the (almost) instantaneous average over an area of about 1000 km^2. Lin *et al.* [7] have shown that notably in the Tropics in convective situations wind variability is high, and that buoy measurements averaged over periods longer than 10 min are more representative for scatterometer winds. However, such an approach is considered outside the scope of this work.

III. WVC Grid Definition

The average distance between two full-resolution measurements in the along-track direction is about 5.6 km, which restricts the WVC grid size to multiples of 5.6 km. Here, we concentrate on a WVC grid size of 5.6 km and refer to the resulting wind product as ASCAT-5.6.

A. Handling of Missing Full-Resolution Data

The full-resolution radar cross-section data provided by EUMETSAT are ordered with antenna pulse time. The antennas are numbered one to six (left fore, left mid, left aft, right fore, right mid, and right aft, respectively). Each antenna at a time emits a pulse and receives its echo that is processed on-board. Also some averaging is done on-board, so a single radar cross-section value is the weighted average of eight antenna pulses [3].

The WVC grid is required to be free of gaps. The first problem encountered when defining a WVC grid synchronized with the ASCAT mid-beam measurements is that sometimes full-resolution data are missing. However, the number of missing antenna pulses can be determined with sufficient accuracy from the time between two pulses of the same antenna, which varies between 0.848 and 0.851 s with an average of about 0.84934 s for gap-free data.

B. Grid Definition and Aggregation Table

The definition of the WVC grid starts with the selection of an aggregation radius. For ASCAT-5.6, a value of 7.5 km is chosen to facilitate comparison with the ASCAT-6.25 product.

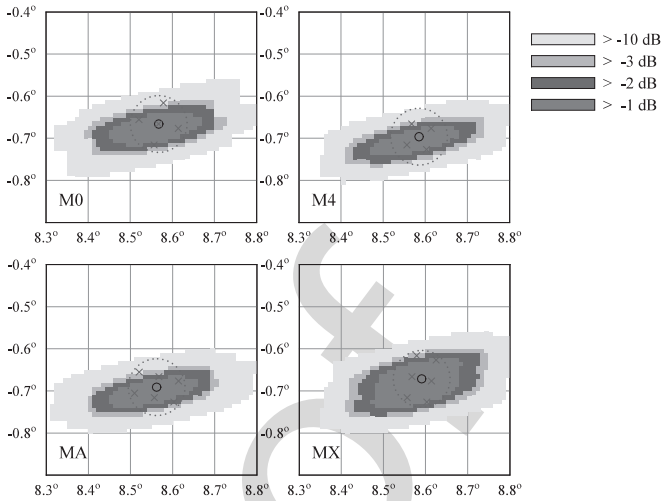

Fig. 3. Mid-beam aggregation patterns and CSRF for the four possible symmetrical ASCAT-5.6 grids at low incidence angle.

As noted above, radar sampling is poorest for the mid beam at low incidence angles. In order to maximize the number of mid-beam full-resolution measurements within the aggregation area, the WVC center must be located symmetrically with respect to them. For a mid-beam synchronized WVC grid, there are four possibilities, as shown in Fig. 3, for an example at lowest incidence angle near the equator: WVC center coinciding with a measurement center (M0, upper left), WVC center in between four measurements (M4, upper right), WVC center between two neighboring measurements in the along-track direction (MA, lower left), and WVC center between two measurements in the cross-track direction (MX, lower right). The full-resolution measurement centers are indicated as crosses in Fig. 3, the WVC center as a small solid circle, and the 7.5 km aggregation area as a larger dotted circle. In color are the values of the CSRF. It is the sum of the SRFs of all contributing measurements, normalized to a maximum value of 1 (0 dB). The SRF's were computed following the approach in [3].

Fig. 3 shows that the MA and MX grids are to be preferred since they contain six measurements in the aggregation area whereas M0 has five and M4 only four. The CSRF for the MX grid has the most circular shape, so this grid is selected.

Next, a row of WVC's with 5.6 km grid size is defined in the mid-beam (cross-track) direction at each side of the satellite track, starting from a particular row of mid-beam full-resolution data. If the distance between the WVC's is kept fixed, the measurement pattern will soon become less optimal, since the measurements are unevenly spaced in the mid-beam direction. Therefore, the MX choice is kept for each WVC, so all WVC centers are located between two neighboring measurements in the cross-track direction. The consequence is that the distance between neighboring WVC's in the cross-track direction is no longer constant.

Finally, the measurements contributing to each WVC in one row are found. Their relative along- and cross-track indices are stored in a look-up table named aggregation table. When deriving ocean surface winds from the radar cross sections, it suffices

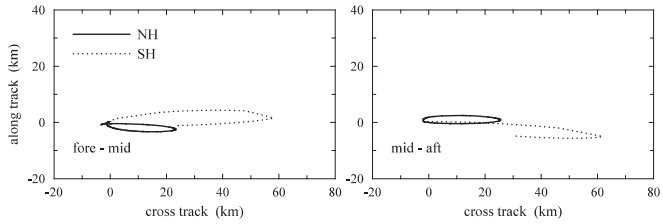

Fig. 4. Libration in along-track versus cross-track distances between fore and mid-beam centers (left-hand panel) and between mid and aft beam centers (right-hand panel). The gap in the Southern Hemisphere (SH) curves (dotted curves) is caused by land overpass.

to read in the full-resolution data and the appropriate aggregation table. The full-resolution cross sections contributing to a particular WVC area are then easily found from the aggregation table. This constitutes a much more efficient algorithm than searching through the full-resolution data for each WVC as implemented in AWDP for ASCAT-coastal and ASCAT-6.25. This is important, since ASCAT-5.6 may have 200 WVC's in a row and over 7100 rows in an orbit.

C. Libration Correction

There is, however, a complication in applying aggregation tables. In order to keep its antennas pointed to the Earth's surface, the Metop platform has to rotate once every orbit around its axis perpendicular to the orbital plane. This rotation has constant angular velocity, but the orbit is slightly elliptical due to the nonuniform mass distribution of the Earth. As a result, the orientation of the Metop platform as viewed from the Earth changes slightly during its orbit, a movement known in astronomy as libration. Fig. 4 shows the along-track and cross-track distances between the left fore and left mid beam (left-hand panel) and between the left mid and left aft beam (right-hand panel), for the lowest incidence angle during one orbit on August 1, 2013. The solid curves pertain to the Northern Hemisphere, the dotted ones to the Southern Hemisphere. The gap in the dotted curves is caused by land overpass. Above the equator—where the aggregation tables were generated—the beams overlap, but over the poles, notably the South Pole, the distance between the beams increases to 60 km.

This can be corrected for by calculating WVC-dependent offsets in the aggregation table for the fore and aft beams, such that these beams overlap as much as possible with the mid beam. Let the central position of each beam in a WVC be defined as the average geographical latitude and longitude of the full-resolution measurements contributing to the radar cross section attributed to that WVC. First consider the fore beam.

Let Δ_A^f be the distance between the measurements in the along-track direction ($\Delta_A^f \approx 5.6$ km) and Δ_R^f that in the range direction. The positive range direction is outward from the satellite. It makes an angle of $\pm 45^\circ$ with the along-track direction, so the projection of Δ_R^f in the cross-track direction is $\delta_X^f = \frac{1}{2}\sqrt{2}\Delta_R^f$ and that in the along-track direction is $\delta_A^f = \frac{1}{2}\sqrt{2}\Delta_R^f$. Fig. 3 shows a schematic representation for the right fore beam. Let d_A^f and d_X^f be the distance between the central positions of fore- and mid beam in the along-track and cross-track directions, respectively. The offsets m_A^f and m_R^f needed to shift the fore beam as close as possible to the mid beam satisfy

$$d_A^f = m_A^f \Delta_A^f + m_R^f \delta_A^f = m^f{}_A \Delta^f{}_A + \tfrac{1}{2}\sqrt{2} m_R^f \Delta_R^f, \quad (1a)$$

$$d_X^f = m_R^f \delta_X^f = \tfrac{1}{2}\sqrt{2} m_R^f \Delta_R^f. \quad (1b)$$

From (1a) and (1b), it immediately follows that

$$m_A^f = \frac{d_A^f - d_X^f}{\Delta_A^f}, \quad m_R^f = \sqrt{2}\frac{d_X^f}{\Delta_R^f}. \quad (2)$$

The aft beam makes an angle of $\pm 135^\circ$ with the along-track direction, so analogous to the above, the projections of Δ_R^a on the cross-track and along-track directions are $\delta_X^a = \frac{1}{2}\sqrt{2}\Delta_R^a$ and $\delta_A^a = -\frac{1}{2}\sqrt{2}\Delta_R^a$. Now the offsets m_A^a and m_R^a must satisfy

$$d_A^a = m_A^a \Delta_A^a + m_R^a \delta_A^a = m_A^a \Delta_A^a - \tfrac{1}{2}\sqrt{2} m_R^a \Delta_R^a, \quad (3a)$$

$$d_X^a = m_R^a \delta_X^a = \tfrac{1}{2}\sqrt{2} m_R^a \Delta_R^a. \quad (3b)$$

This is solved as

$$m_A^a = \frac{d_A^a + d_X^a}{\Delta_A^a}, \quad m_R^a = \sqrt{2}\frac{d_X^a}{\Delta_R^a}. \quad (4)$$

Of course the offsets are integers, so the expressions in the right-hand sides of (2) and (4) are rounded off to the nearest integer. The procedure must be iterated because the along-track and cross-track measurement distances Δ_A and Δ_R are not constant over the swath, notably Δ_R at low incidence. This iteration converges in a few steps and does not add much to the processing time.

D. Manual Editing of the Aggregation Table

The libration correction must be done for every WVC. Therefore, the aggregation table does not need to be very precise, as any mismatch between the beams will be compensated for as good as possible. As a consequence, the aggregation table can be edited manually for, say, the left fore and left mid beam, and defined for the other beams symmetrically with respect to the along-track and cross-track directions.

E. Grids Used

In this paper, two ASCAT-5.6 products will be studied. The first product is obtained by using an aggregation table constructed for one row of WVC's and for each beam separately by aggregating the measurements in a circular aggregation area with 7.5 km radius. This is equivalent to ASCAT-6.25 sampling, except that the same aggregation table is used for all rows of WVC's, resulting in more uniform radar sampling. This product will be further referred to as (ordinary) ASCAT-5.6.

The second product is obtained by manually adding measurements to the aggregation table in such a way that the -3 dB contours of the resulting CSRF's for the left fore and left mid-beam cover as good as possible the aggregation area with radius 7.5 km. For the left fore beam there are two patterns, one for WVC's 1 to 65 and one for WVC's 66 to 100. For the

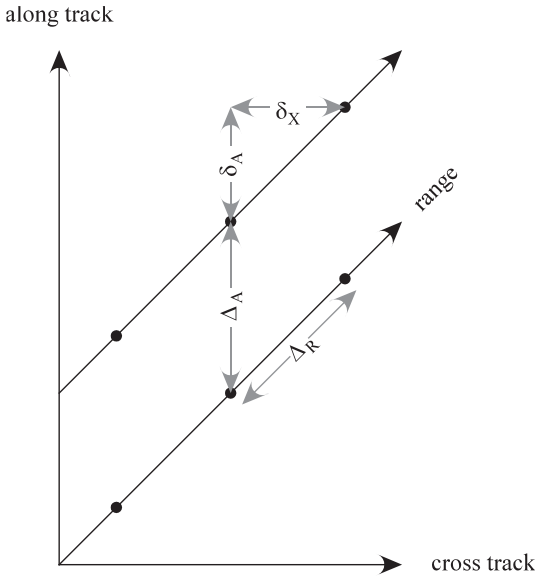

Fig. 5. Geometry for libration correction of the right fore beam. The solid dots indicate the footprint centers of the right fore beam.

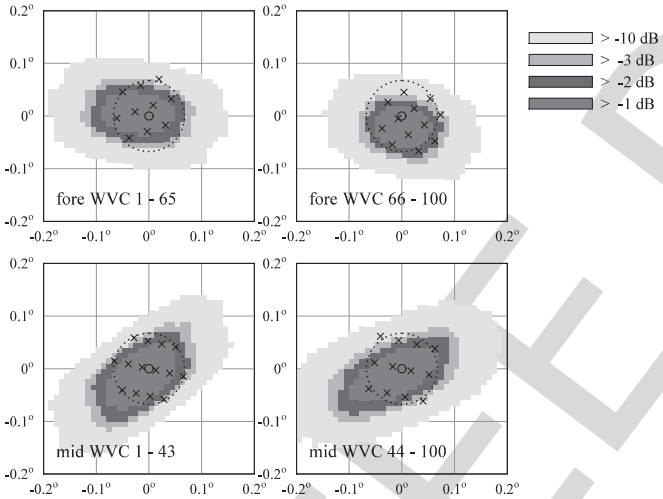

Fig. 6. Aggregation patterns for the improved ASCAT-5.6 product.?>

left mid beam there are also two patterns, one for WVC's 1 to 43 and one for WVC's 44 to 100. Fig. 6 shows the aggregation patterns used for the left fore and left mid beams. The contributing measurements are indicated by crosses, the WVC center by the small solid circle, and the edge of the aggregation area with 7.5 km radius by the dotted circle. The CSRFs in Fig. 6 are for WVCs 32 (upper left panel), 84 (upper right panel), 22 (lower left panel), and 72 (lower right panel), halfway in the range of validity of the aggregation pattern. The aggregation table for the other beams is defined symmetrically with respect to the along-track and cross-track directions. This product will be referred to as improved ASCAT-5.6.

From Fig. 6, it is clear that it is not easy to define circular CSRFs, because of the elongated elliptical shape of the SRFs (see also Fig. 2). Comparison of Fig. 6 with Fig. 3 shows that the improved product has twice as many contributing

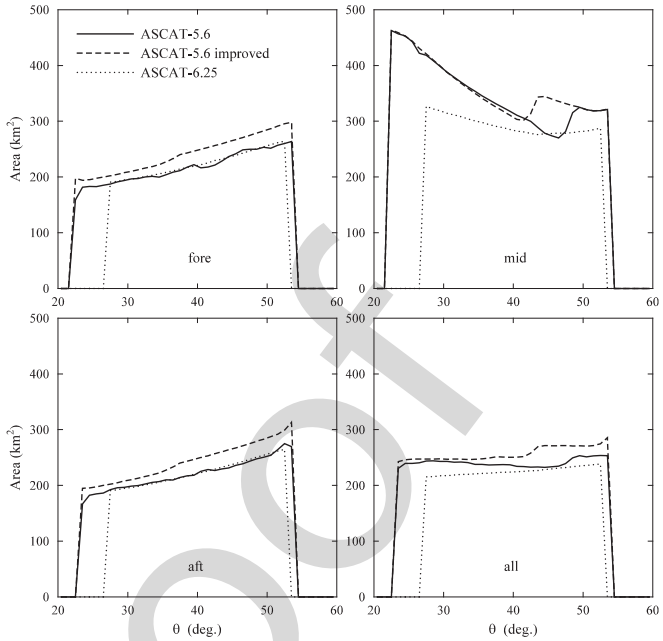

Fig. 7. Area covered by the −3 dB contour of the CSRF versus incidence angle.

measurements in the mid beam at low incidence than the ordinary ASCAT-5.6 product.

IV. Results

A. Spatial Resolution and Overlap

Fig. 7 shows the area covered within the −3 dB contour of the CSRF for the two products defined in the previous section and for ASCAT-6.25 as a function of incidence angle. The results in Fig. 5 are based on data from one orbit on August 16, 2013. The improved ASCAT-5.6 product has the largest area, notably in the mid beam at small incidence angle. This is as expected, because the improved grid was defined to have as much SRFs as possible contributing to a WVC. The ordinary ASCAT-5.6 product has larger area than the ASCAT-6.25 product in the mid beam, but not in the fore and aft beams. This is because ASCAT-5.6 uses the same optimal aggregation pattern for the mid beam, so the number of contributing mid-beam SRFs is constant for each WVC. For ASCAT-6.25, this number varies along the swath, and also less mid-beam SRFs may contribute to a WVC, leading to a −3 dB CSRF area that is smaller than that of ASCAT-5.6. For the fore and aft beams, sampling is less critical, so the differences between the three products are smaller.

The mid-beam area decreases with increasing the incidence angle, while the fore and aft beam areas increase. As a result, the −3 dB CSRF area for all beams (lower right panel of Fig. 7) varies little with incidence angle. Assuming the −3 dB contour of the all-beams CSRF area to be circular, the diameter of this circle is 19 km for the improved ASCAT-5.6 product, 18 km for the ordinary ASCAT-5.6 product, and 17 km for the ASCAT-6.25 product. These values are adopted as measures of the true spatial resolution.

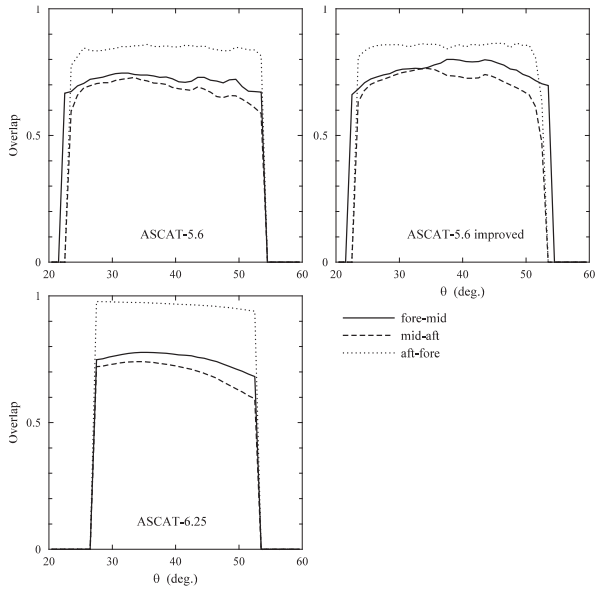

Fig. 8. Overlaps between the three beam pairs as a function of incidence angle.

Despite the fact that the two ASCAT-5.6 products have larger CSRFs per beam, their overall true spatial resolution is almost the same as that of ASCAT-6.25. This is caused by the fact that each of the three beams illuminates a slightly different area. As a result, the all beam CSRF has a narrow peak, yielding good spatial resolution, but also a long tail, enhancing geophysical errors. This can be understood from the beam overlap. The overlap $O_{\alpha\beta}$ between beams α and β is defined as in [1]

$$O_{\alpha\beta} = \frac{I_{\alpha\beta}^2}{I_{\alpha\alpha} I_{\beta\beta}} \tag{5}$$

with

$$I_{\alpha\beta} = \int\int d\lambda d\varphi \, \cos\varphi \, C_\alpha(\lambda,\varphi) \, C_\beta(\lambda,\varphi) \tag{6}$$

where C_α stands for the CSRF of beam α as a function of geographical longitude λ and latitude φ, and the integration is over the entire domain of the CSRFs.

Fig. 8 shows the overlap between the three beam pairs for the two ASCAT-5.6 products and ASCAT-6.25 as a function of incidence angle. Fig. 8 is based on data from the same orbit as used for Fig. 7. The overlap between the fore and aft beam of the ordinary and improved ASCAT-5.6 products is worse than that of ASCAT-6.25. This is due to the fact that the libration correction is discrete, so it is unable to shift the fore and aft beam centers exactly on the mid-beam center. On the other hand, the improved ASCAT-5.6 has slightly better overlap between fore and mid beam and between mid and aft beam than ASCAT-6.25. This is because the mid-beam CSRF is better defined.

B. Buoy Comparison

The ASCAT winds were collocated with buoys. Table I shows the standard deviation of the difference between scatterometer and buoys for wind speed, wind direction, zonal wind component u, and meridional wind component v. Only collocations common to all three datasets were considered, resulting in 2475 collocations. Wind direction statistics were only considered in case all wind speeds exceeded 4 m/s, resulting in 1712 collocations. The accuracies in the bottom row are based on the inverse square root of the number of collocations.

TABLE I
BUOY COMPARISON

Product	σ_s (m/s)	σ_d (deg)	σ_u (m/s)	σ_v (m/s)
ASCAT-6.25	0.99	17.3	1.48	1.61
ASCAT-5.6	1.00	17.3	1.46	1.65
ASCAT-5.6 Improved	0.99	16.8	1.45	1.61
Accuracy	0.02	0.4	0.03	0.03

Table I shows that there is little difference between ASCAT-6.25 and ASCAT-5.6, though the agreement for u is slightly better and that for v is slightly worse. The improved ASCAT-5.6 product compares best with buoys, in particular for the wind direction. This indicates that manual editing of the aggregation tables for the left-fore and left-mid beam and symmetric definition of the other beams indeed leads to a better product. In particular, the doubling of the number of contributing measurements in the mid beam at low incidence angles leads to less noise in the radar cross sections, and hence better wind retrievals.

Nevertheless, Table I shows that the differences are on the edge of being significant, and more work on much larger datasets remains to be done in order to reduce statistical uncertainty.

C. Some Examples

Fig. 9 shows improved ASCAT-5.6 (upper panel) and ASCAT-6.25 (lower panel) wind fields of a frontal zone south of Australia recorded by ASCAT-A on July 31, 2013 (orbit starting at 22:42 UTC). Blue arrows denote valid winds and purple arrows winds flagged by the variational QC. The latter control flag is set when the mismatch between scatterometer observation and background wind field exceeds a certain limit. This is often caused by mispositioning of mesoscale wind structures in the background. Fig. 9 shows some ambiguity removal errors in the frontal zone as encircled arrows. The ASCAT-6.25 scene contains 11 clear ambiguity removal errors; the improved ASCAT-5.6 scene 9, despite its higher density of retrieved winds. Though there may be discussion on the exact number of ambiguity removal errors—only the most obvious ones were marked in Fig. 7—the improved ASCAT-5.6 product contains less errors than the ASCAT-6.25 product. In particular, the two ambiguity removal errors in the ASCAT-6.25 product near the 138° meridian have disappeared in the improved ASCAT-5.6 product. Note also that all ambiguity removal errors in the scene are flagged in the improved ASCAT-5.6 product, but not in the ASCAT-6.25 product.

Another example is given by Fig. 10, which shows a convective area in the Tropical western Pacific recorded by ASCAT-A

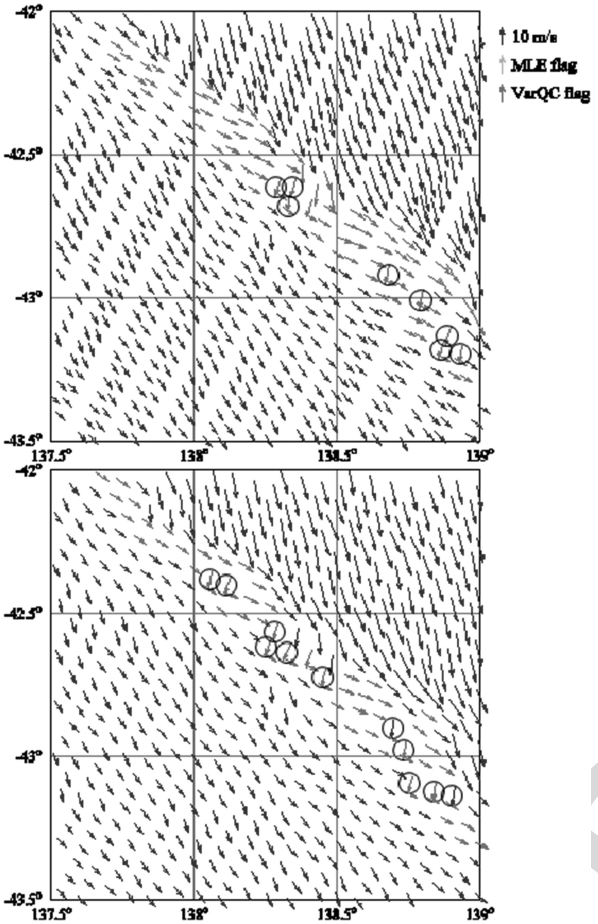

Fig. 9. Improved ASCAT-5.6 (upper panel) and ASCAT-6.25 (lower panel) wind fields over a frontal zone south of Australia recorded July 31, 2013. Wind vectors with obvious ambiguity removal errors have been encircled.

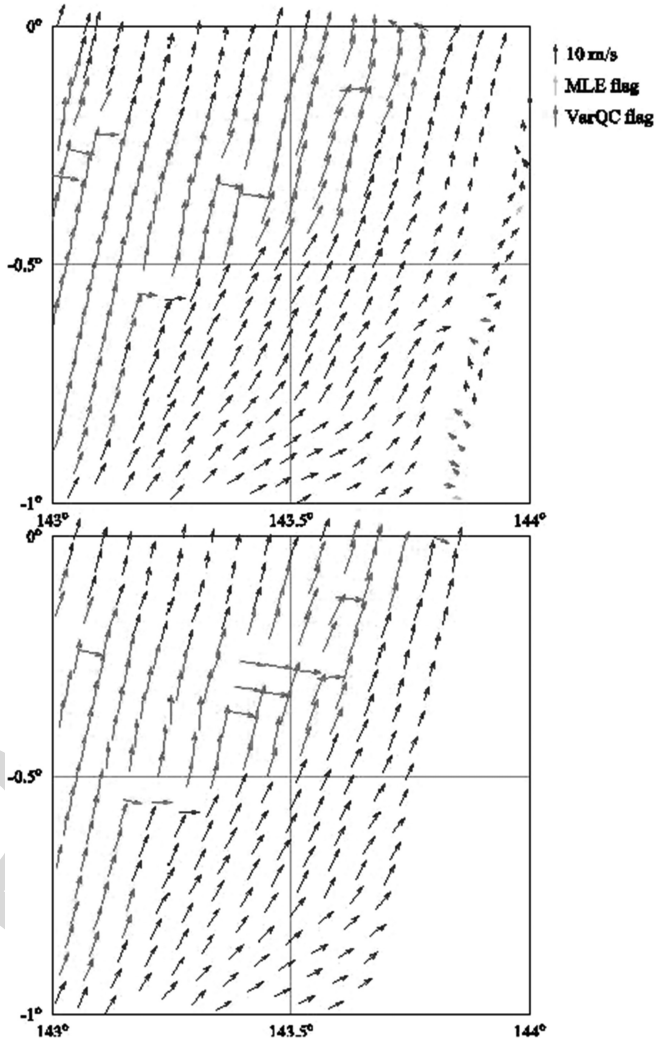

Fig. 10. Improved ASCAT-5.6 (upper panel) and ASCAT-6.25 (lower panel) wind fields over a convective area in the Tropical western Pacific recorded August 2, 2013.

on August 2, 2013 shortly after 0:00. The flow is from South to North, but ambiguity removal errors cause some wind vectors to point to the West. These are easy to recognize, so they have not been marked. The top panel, showing improved ASCAT-5.6 data, contains 8 ambiguity removal errors, while the bottom panel, showing ASCAT-6.25, contains 13. As in Fig. 9, the variational QC flag is set in a number of WVCs (purple arrows), caused by poor representation of the convective mesoscale structure in the ECMWF background wind field.

Note that the improved ASCAT-5.6 scene in Fig. 10 covers a larger area than the ASCAT-6.25 scene, because it has extra WVCs at the Eastern side of the swath, where the incidence angle is highest. This is because ASCAT-5.6 processing accepts measurements at higher incidence angles than ASCAT-6.25 processing. The quality of these additional retrievals is poor, so an operational product should better not contain them, either by limiting the incidence angle range or by improving QC.

V. Discussion

The results in Section IV show that it is indeed possible to define an ASCAT wind product on a 5.6 km grid synchronized with the ASCAT mid-beam pattern with better quality than the ASCAT-6.25 product, though at the cost of a slightly reduced true spatial resolution (19 km against 17 km) and irregular grid size.

However, the possibilities for defining the WVC grid and the aggregation pattern are far from exhausted. The MX grid in Fig. 3 leads to a more circular CSRF than the MA grid, but the MA grid has a more compact CSRF. Manual editing of the MA aggregation table may lead to better results.

In the products, presented in this study, it was attempted to retain a rectangular WVC grid with the same size in along-track and cross-track directions as much as possible. The requirement that the mid-beam center should fall exactly between two measurements in the cross-track directions leads to nonuniform grid sizes in the cross-track direction, see Figs. 9 and 10. Another possibility is to synchronize the grid in the cross-track direction also with the mid-beam measurement pattern. One may select a suitable aggregation pattern for the left fore and left mid beams, define those for the other beams symmetrically with respect to the along-track and cross-track directions, and apply the

aggregation pattern every *n*th measurement in the range direction. This will lead to a product with constant radar sampling characteristics, but different grid sizes in along-track and cross-track directions. Moreover, the grid size in the cross-track direction will vary with the incidence angle: it will be larger at small incidence and smaller at large incidence. The same holds for the true spatial resolution. Such a product will be more comfortable to the eye than the improved ASCAT-5.6 products shown in Figs. 9 and 10. More investigations are needed to assess the quality of such products, and extensive interactions with potential end users are required to arrive at products that suit their needs.

The elliptical shape of the individual SRFs (see Fig. 2) poses a lower limit on the true spatial resolution that can be obtained, in particular at low incidence angles. The possibility to define a wind product with optimized true spatial resolution at intermediate and high incidence, at the cost of noisier winds, also remains to be investigated.

In this study, the high-resolution wind products were compared with buoy winds averaged over 10 min. As has been shown in [7], it is better to compare with buoy winds averaged over a longer time period that is centered around the scatterometer measurement time. At 7 m/s wind speed, buoy measurements over 10 min are representative for a scale of about 4 km, which is much smaller than the area covered by a scatterometer WVC. This is also a subject for further research.

A final remark pertains the successors of the present series of ASCAT instruments that will be mounted on the second generation of polar-orbiting Metop satellites (Metop-SG) from 2022 onwards. These will have no on-board averaging, resulting in a denser measurement pattern and SRFs with a more circular shape, offering even more possibilities to define ultrahigh-resolution wind products.

VI. Conclusion

In this study, two new high-resolution ASCAT wind products on a 5.6 km grid were compared to the ASCAT-6.25 product. The ASCAT-5.6 grid is synchronized to the ASCAT mid-beam measurements, and the cross-track grid position is determined by the requirement that it should fall exactly between two consecutive measurements. This leads to nonuniform grid sizes in the cross-track direction. A very efficient processing scheme is arrived at by using aggregation tables in combination with a libration correction.

The ordinary ASCAT-5.6 product is similar to the ASCAT-6.25 product, but with constant radar sampling. The improved ASCAT-5.6 product employs an aggregation table that has been edited manually to maximize the number of contributing measurements.

The true spatial resolution is defined as the diagonal of the -3 dB contour of the all-beams CSRF. For the ASCAT-6.25, ASCAT-5.6, and improved ASCAT-5.6 products it is 17, 18, and 19 km, respectively. The ASCAT-5.6 products have poorer overlap between the beams than the ASCAT-6.25 product, because the libration correction is discrete. The improved ASCAT-5.6 product compares better with buoys than the other two products, because the increased number of measurements contributing to a WVC leads to better quality winds. This is confirmed by a few examples showing less ambiguity removal errors in the improved ASCAT -5.6 product than in the ASCAT-6.25 product. It is concluded that the improved ASCAT-5.6 product has better quality than the ASCAT-6.25 product, at the cost of a slightly inferior true spatial resolution.

No QC of the inversion was considered here, but generally a more consistent retrieval also provides a more consistent QC. This needs verification in future work.

The ASCAT-5.6 wind products presented in this study are the first to exploit the possibilities offered by the full-resolution product. A number of options remains to be investigated, and extensive interaction with end users will be required to arrive at wind products that suit their needs.

References

[1] J. Vogelzang, A. Stoffelen, R. Lindsley, A. Verhoef, and J. Verspeek, "The ASCAT-6.25-km product," *IEEE J. Sel. Topics Remote Sens.*, 2016, doi: 10.1109/JSTARS.2016.2623862

[2] A. Verhoef, M. Portabella, and A. Stoffelen, "High-resolution ASCAT scatterometer winds near the coast," *IEEE Trans. Geosci. Remote Sens.*, vol. 50, no. 7, pp. 2481–2487, Jul. 2012, doi:10.1109/TGRS.2016.2544835

[3] R. D. Lindsley, C. Anderson, J. Figa-Saldaña, and D. Long, "A parameterized ASCAT measurement spatial response function," *IEEE Trans. Geosci. Remote Sens.*, vol. 54, no. 8, pp. 4570–4579, Aug. 2016. doi:10.1109/TGRS.2016.2544835

[4] *ASCAT* Wind Product User Manual, KNMI, De Bit, The Netherlands, 2013. [Online]. Available: http://projects.knmi.nl/ scatterometer/publications/pdf/ASCAT_Product_Manual.pdf

[5] J. Bidlot, D. Holmes, P. Wittmann, R. Lalbeharry, and H. Chen, "Intercomparison of the performance of operational ocean wave forecasting systems with buoy data," *Weather Forecasting*, vol. 17, pp. 287–310, 2002, doi:10.1175/1520-0434(2002)017<0287:IOTPOO>2.0.CO;2

[6] W. T. Liu, K. B. Katsaros, and J. A. Businger, "Bulk parameterization of air-sea exchanges of heat and water vapor including the molecular constraints in the interface," *J. Atmos. Sci.*, vol. 36, pp. 1722–1735, 1979, doi:10.1175/1520-0469(1979)036<1722:BPOASE>2.0.CO;2

[7] W. Lin, M. Portabella, A. Stoffelen, A. Verhoef, and A. Turiel, "ASCAT wind quality control near rain," *IEEE Trans. Geosci. Remote Sens.*, vol. 53, no. 8, pp. 4165–4177, Aug. 2015.

Jur Vogelzang was born in The Netherlands in 1955. He received the M.Sc. degree in theoretical physics from the Free University, Amsterdam, The Netherlands, in 1981, and the Ph.D. degree in physics on radar remote sensing from the University of Utrecht, Utrecht, The Netherlands, in 1998.

He is currently with the Royal Netherlands Meteorological Institute (KNMI), De Bilt, The Netherlands, where he is working on scatterometer wind products.

Ad Stoffelen was born in 1962 in The Netherlands. He received the M.Sc. degree in physics from the Technical University of Eindhoven, Eindhoven, The Netherlands, in 1987, and the Ph.D. degree in meteorology on scatterometry from the University of Utrecht, Utrecht, The Netherlands.

He currently leads a group on active satellite sensing at KNMI and is involved in topics from future missions and retrieval to 24/7 operations, user training and services. He is also deeply involved in the European Space Agency ADM-Aeolus Doppler Wind Lidar mission.